Quaternary Science Reviews 77 (2013) 167–180

Contents lists available at ScienceDirect

Quaternary Science Reviews

journal homepage: www.elsevier.com/locate/quascirev

A 500,000 year record of Indian summer monsoon dynamics recorded by eastern equatorial Indian Ocean upper water-column structure

Clara T. Bolton [a,*], Liao Chang [a,1], Steven C. Clemens [b], Kazuto Kodama [c], Minoru Ikehara [c], Martin Medina-Elizalde [a,2], Greig A. Paterson [a,3], Andrew P. Roberts [a,1], Eelco J. Rohling [a,1], Yuhji Yamamoto [c], Xiang Zhao [a,1]

[a] School of Ocean and Earth Science, National Oceanography Centre, University of Southampton, Southampton SO14 3ZH, United Kingdom
[b] Department of Geological Sciences, Brown University, Providence, RI, USA
[c] Center for Advanced Marine Core Research, Kochi University, Kochi, Japan

ARTICLE INFO

Article history:
Received 1 February 2013
Received in revised form
4 July 2013
Accepted 22 July 2013
Available online

Keywords:
Monsoon
Indian Ocean
Stratification
Wind
Precession
Half-precession
Millennial

ABSTRACT

The Indian Summer Monsoon (ISM) is an inter-hemispheric and highly variable ocean–atmosphere–land interaction that directly affects the densely populated Indian subcontinent. Here, we present new records of palaeoceanographic variability that span the last 500,000 years from the eastern equatorial Indian Ocean, a relatively under-sampled area of ISM influence. We have generated carbon and oxygen stable isotope records from three foraminiferal species from Ocean Drilling Program Site 758 (5°N, 90°E) to investigate the oceanographic history of this region. We interpret our resultant $\Delta\delta^{18}O$ (surface-thermocline) record of upper water-column stratification in the context of past ISM variability, and compare orbital phase relationships in our Site 758 data to other climate and monsoon proxies in the region. Results suggest that upper water-column stratification at Site 758, which is dominated by variance at precession and half-precession frequencies (23, 19 and 11 ka), is forced by both local (5°N) insolation and ISM winds. In the precession (23 ka) band, stratification minima at Site 758 lag northern hemisphere summer insolation maxima (precession minima) by 9 ka, which is consistent with Arabian Sea ISM phase estimates and suggests a common wind forcing in both regions. This phase implicates a strong sensitivity to both ice volume and southern hemisphere insolation forcing via latent heat export from the southern subtropical Indian Ocean. Additionally, we find evidence of possible overprinting of millennial-scale events during glacial terminations in our stratification record, which suggests an influence of remote abrupt climate events on ISM dynamics.

1. Introduction

The south Asian, or Indian, summer monsoon, a subsystem of the Asian summer monsoon, is a large-scale, highly dynamic ocean–atmosphere–land interaction centred on the Indian subcontinent, which affects crop production and the livelihoods of over a billion people (e.g. Webster et al., 1998; Ding and Chan, 2005; Wang et al., 2005). The Indian summer monsoon (ISM) is driven by asymmetric heating between the cooler Indian Ocean and the warmer Indo-Asian landmasses such that, during boreal summer (May–September), intense heating results in a strong pressure gradient between Asia (low pressure) and the southern subtropical Indian Ocean (SSIO, high pressure) that leads to large-scale shifts in the position of the Intertropical Convergence Zone (ITCZ). Low pressure over Asia is driven by both sensible (direct) heating of the Asian landmass and latent (condensational) heating in the overlying troposphere. Latent heat that originates from evaporation of surface waters over the SSIO is transported northward as moisture-rich winds toward the high-altitude Himalayas, where it is released as precipitation, which further enhances low pressure over Asia during the summer monsoon (Krishnamurti, 1985; Webster, 1987; Clemens et al., 1991; Webster et al., 1998; Schott and McCreary, 2001; Shankar et al., 2002; Gadgil, 2003; Wang et al., 2003a; Gadgil et al., 2007).

* Corresponding author. Present address: Geology Department, University of Oviedo, Arias de Velasco SN, 33005 Oviedo, Asturias, Spain. Tel.: +34 985103165.
E-mail addresses: cbolton@geol.uniovi.es, ctb101@gmail.com (C.T. Bolton).
[1] Present address: Research School of Earth Sciences, The Australian National University, Canberra, ACT 0200, Australia.
[2] Present address: Centro de Investigación Científica de Yucatán, UCIA, Cancún, Mexico.
[3] Present address: Key Laboratory of Earth's Deep Interior, Institute of Geology and Geophysics, Chinese Academy of Sciences, Beijing 100029, China.

0277-3791/$ – see front matter © 2013 Elsevier Ltd. All rights reserved.
http://dx.doi.org/10.1016/j.quascirev.2013.07.031

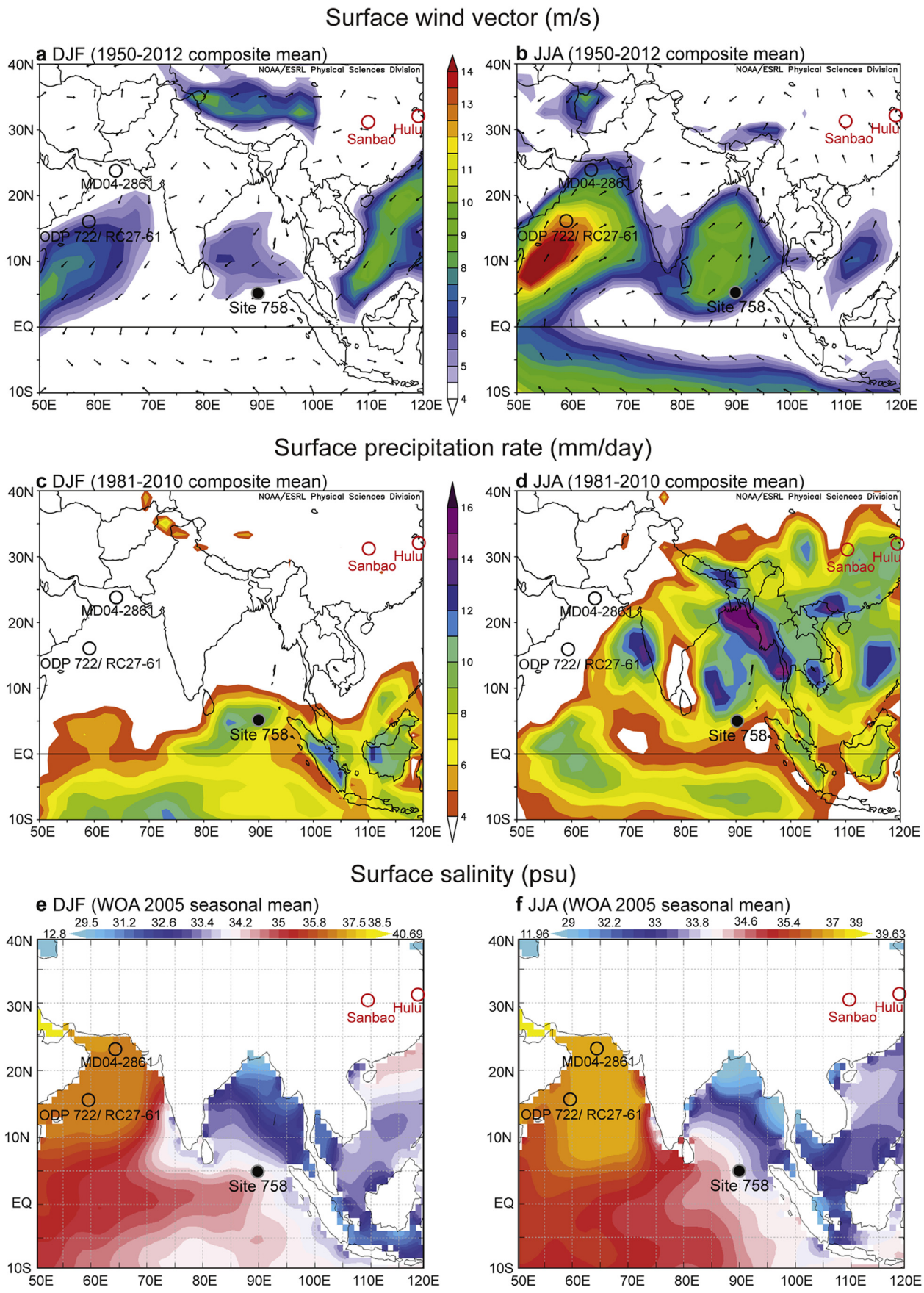
Surface wind vector (m/s)
a DJF (1950-2012 composite mean)
b JJA (1950-2012 composite mean)
NOAA/ESRL Physical Sciences Division
Sanbao
Hulu
MD04-2861
ODP 722/ RC27-61
Site 758
40N
30N
20N
10N
EQ
10S
50E
60E
70E
80E
90E
100E
110E
120E
14
13
12
11
10
9
8
7
6
5
4
Surface precipitation rate (mm/day)
c DJF (1981-2010 composite mean)
d JJA (1981-2010 composite mean)
16
14
12
10
8
6
4
Surface salinity (psu)
e DJF (WOA 2005 seasonal mean)
12.8
29.5
31.2
32.6
33.4
34.2
35
35.8
37.5
38.5
40.69
f JJA (WOA 2005 seasonal mean)
11.96
29
32.2
33
33.8
34.6
35.4
37
39
39.63

The ISM system varies over a wide range of timescales. The expression of variations in summer monsoon winds and precipitation in palaeoclimate archives as well as past variations in ISM intensity on suborbital to tectonic timescales are understood to a large degree thanks to numerous proxy reconstructions from the Arabian Sea (Prell, 1984; Prell et al., 1989; Clemens and Prell, 1990, 2003, 2007; Clemens et al., 1991, 1996; Altabet et al., 1995, 1999; Reichart et al., 1998; Schulz et al., 1998; Burns et al., 2003, 2004; Leuschner and Sirocko, 2003; Wang et al., 2005; Ishikawa and Oda, 2007; Govil and Naidu, 2010; Bassinot et al., 2011; Caley et al., 2011a, 2011b), the South China Sea (Chen et al., 2003), the Bay of Bengal (Kudrass et al., 2001; Rachid et al., 2011) and the equatorial Indian Ocean (Chen and Farrell, 1991; Beaufort et al., 1997; Gupta and Mélice, 2003; Rachid et al., 2007; Bassinot et al., 2011; Caley et al., 2011c). Model simulations have also advanced our understanding of the ISM system (Prell and Kutzbach, 1992; Kutzbach et al., 1993, 2008; Wright et al., 1993; Masson et al., 2000; Levermann et al., 2009; Ziegler et al., 2010). Despite this effort, significant uncertainties remain with respect to the degree of coupling between the Asian monsoon sub-systems (i.e. East Asian and Indian), the physical aspects of monsoon-related variability recorded by proxies in different regions (e.g. wind-driven upwelling strength versus changes in nutrient content of upwelled water, versus precipitation over the continents) and the extent to which forcing mechanisms and Earth-orbital phase relationships are common between monsoon systems (Ruddiman, 2006; Clemens and Prell, 2007; Wang et al., 2008; Clemens et al., 2010; Ziegler et al., 2010; Caley et al., 2011b). Large discrepancies exist between phase estimates of ISM variability relative to climatic precession-driven insolation changes determined in model simulations (ISM maxima in phase with precession (P) minima; Kutzbach et al., 2008; Ziegler et al., 2010; Weber and Tuenter, 2011) and those derived from marine proxy records (8–9 ka phase lag of Arabian Sea proxies relative to P minima; Caley et al., 2011b; Clemens et al., 2008; Clemens and Prell, 2003; Wang et al., 2005). This discrepancy has led to the hypothesis that Arabian Sea palaeoproductivity is influenced by circulation and nutrient delivery changes, as well as ISM variability, on orbital timescales (Ziegler et al., 2010). However, this hypothesis does not account for the similar phase of lithogenic grain size proxies (related to wind strength) that have the same phase as the ocean palaeoproductivity proxies yet are not influenced by ocean nutrient supply.

Here, we present new records of palaeoceanographic variability from the eastern equatorial Indian Ocean, a relatively undersampled area of ISM influence. Carbon and oxygen stable isotope records from three co-existing foraminiferal species from a single core, Ocean Drilling Program (ODP) Hole 758C, spanning the last 500,000 years (500 ka), were generated to investigate the oceanographic history of this important region. Coccolith relative abundance data were also generated to supplement foraminiferal records during discrete intervals. We use the planktic foraminiferal species *Globigerinoides ruber* (white) and *Neogloboquadrina dutertrei*, which are recorders of upper mixed layer and thermocline conditions, respectively, to construct a $\Delta\delta^{18}O$ record ($\delta^{18}O_{G.\ ruber}$ minus $\delta^{18}O_{N.\ dutertrei}$, hereafter $\Delta\delta^{18}O_{r-d}$). In conjunction with a benthic stable isotope record for *Cibicidoides wuellerstorfi*, we establish orbital-scale phase relationships between deep, thermocline and surface-waters at Site 758. On this basis, we examine the potential mechanisms driving $\Delta\delta^{18}O_{r-d}$, which is interpreted as representing upper water-column stratification, and its relationship to existing proxy records of summer monsoon variability in the surrounding regions and their phasing relative to insolation forcing.

2. Site description & oceanographic setting

ODP Site 758 was cored during Leg 121 on Ninety east Ridge (5°23.05′ N, 90°21.67′ E, water depth 2924 m), in the southernmost Bay of Bengal (BOB), equatorial Indian Ocean (Fig. 1). Pleistocene sediments at Site 758 are dominated by well-preserved biogenic calcareous ooze (Shipboard Scientific Party et al., 1989). Oceanographic conditions in the BOB are dominated by seasonal monsoon circulation patterns. Massive freshwater discharge from the major Indian river systems into the northern BOB during the summer months induces a large reduction in sea surface salinity (SSS) and a strong NE-SW salinity gradient (~20–34 psu), with Site 758 at the distal end of this gradient (Antonov et al., 2010, Fig. 1f). Seasonal sea surface temperature (SST) variability in the BOB is relatively small, with the lowest SSTs (~26 °C) recorded in the northern region during winter and near isothermal warm SSTs throughout the BOB during summer (~28–29 °C) (Locarnini et al., 2010). In the surface waters overlying Site 758, SST and SSS are relatively constant throughout the year (~28–29 °C and 34 psu). However, surface wind and current speed and direction change significantly on seasonal timescales throughout the entire BOB, with strong southwesterlies during the summer monsoon and weaker northeasterlies during the winter months. Average surface wind speeds are twice as high during summer (mean June, July, August; JJA) compared to winter (mean December, January, February; DJF) at Site 758 (Fig. 1a and b). Thus, changes in upper water column structure and stratification in this region are dominated by wind-driven mixing rather than salinity or temperature. These stratification changes can be monitored through the oxygen isotopic gradient between shallow- and deep-dwelling foraminifera.

3. Methods

Sediment U-channels, which had previously been subjected to palaeomagnetic analyses, from sections 1–6 of ODP Hole 758C Core 1 were cut into 0.5 cm-thick contiguous slices and were sampled for stable isotope analysis at 2.5 or 5 cm stratigraphic intervals. A toothpick sample was taken for nannofossil analysis, and bulk samples were washed through a 63 μm sieve with tap water then oven dried overnight at 50 °C. In general, three to five specimens of *C. wuellerstorfi* were picked from the >150 μm size fraction for $\delta^{13}C$ and $\delta^{18}O$ analysis. Benthic foraminiferal samples were analysed at the Department of Geological Sciences, Brown University, on a Finnigan MAT 252 dual-inlet isotope ratio mass spectrometer (DI-IRMS) with an automated Kiel III carbonate device. Long-term analyses of internal marble standards calibrated to NBS-19 indicate a routine precision of 0.03‰ for $\delta^{13}C$ and 0.06‰ for $\delta^{18}O$ (1σ). Approximately 30 specimens each of *G. ruber* (white) and *N. dutertrei* were picked from the 212–300 μm and 250–300 μm size fractions, respectively. Only specimens of the *G. ruber* morphotype *sensu stricto* (Wang, 2000; Aurahs et al., 2011) were selected in order to produce the shallowest possible mixed layer

Fig. 1. Seasonal oceanography and location of ODP Site 758 (filled circle) and other sites discussed in the text. Hulu and Sanbao caves, Southeast China (red open circles (Cheng et al., 2009)); Arabian Sea stacks (open black circles, core MD04-2861 (Caley et al., 2011b) and cores ODP Site 722B and RC27-61 (Clemens and Prell, 2003)). (a) and (b) Mean surface wind speed for NH winter (December, January, February; DJF) and summer (June, July, August; JJA), respectively. (c) and (d) Mean precipitation rate for NH winter and summer, respectively. (e) and (f) Mean salinity for NH winter and summer, respectively (note slightly different scales). Maps were created at http://www.esrl.noaa.gov/psd/cgi-bin/data/getpage.pl and http://ferret.pmel.noaa.gov/LAS/. (For interpretation of the references to colour in this figure legend, the reader is referred to the web version of this article.)

signal. Planktic foraminiferal samples were crushed with a needle, ultrasonicated in methanol for 5 s, rinsed in ultrapure MilliQ water then dried at 50 °C prior to analysis. Stable isotope analyses on planktic samples were carried out at the Center for Advanced Marine Core Research, Kochi University, on an IsoPrime DI-IRMS connected to an automated carbonate preparation system with long-term analytical precision of 0.03‰ for $\delta^{13}C$ and 0.06‰ for $\delta^{18}O$.

Samples of *C. wuellerstorfi*, *G. ruber* and *N. dutertrei* were picked and analysed at 2.5 cm resolution over the upper 3 m of the core, and at 5 cm resolution down to 9 m. During select interglacial intervals in the deeper sections, planktic foraminifera were scarce. In cases where insufficient individuals were present in the original selected sample, the sample 2.5 cm deeper and/or shallower was also picked, and one of these individual samples usually yielded enough individuals for an analysis. We did not combine foraminifera from consecutive samples. *C. wuellerstorfi* is an epibenthic foraminiferal species, and we adjusted measured $\delta^{18}O$ values to equilibrium by adding 0.64‰ (Shackleton and Hall, 1984). We constructed an age model via manual graphical correlation of the Site 758C *C. wuellerstorfi* $\delta^{18}O$ record to the LR04 global benthic $\delta^{18}O$ stack (Lisiecki and Raymo, 2005) using Analyseries (Paillard et al., 1996) (correlation = 0.93). This yielded sedimentation rates between ~0.5 and 4 cm/ka (Fig. 2). The age of the Toba ash layer

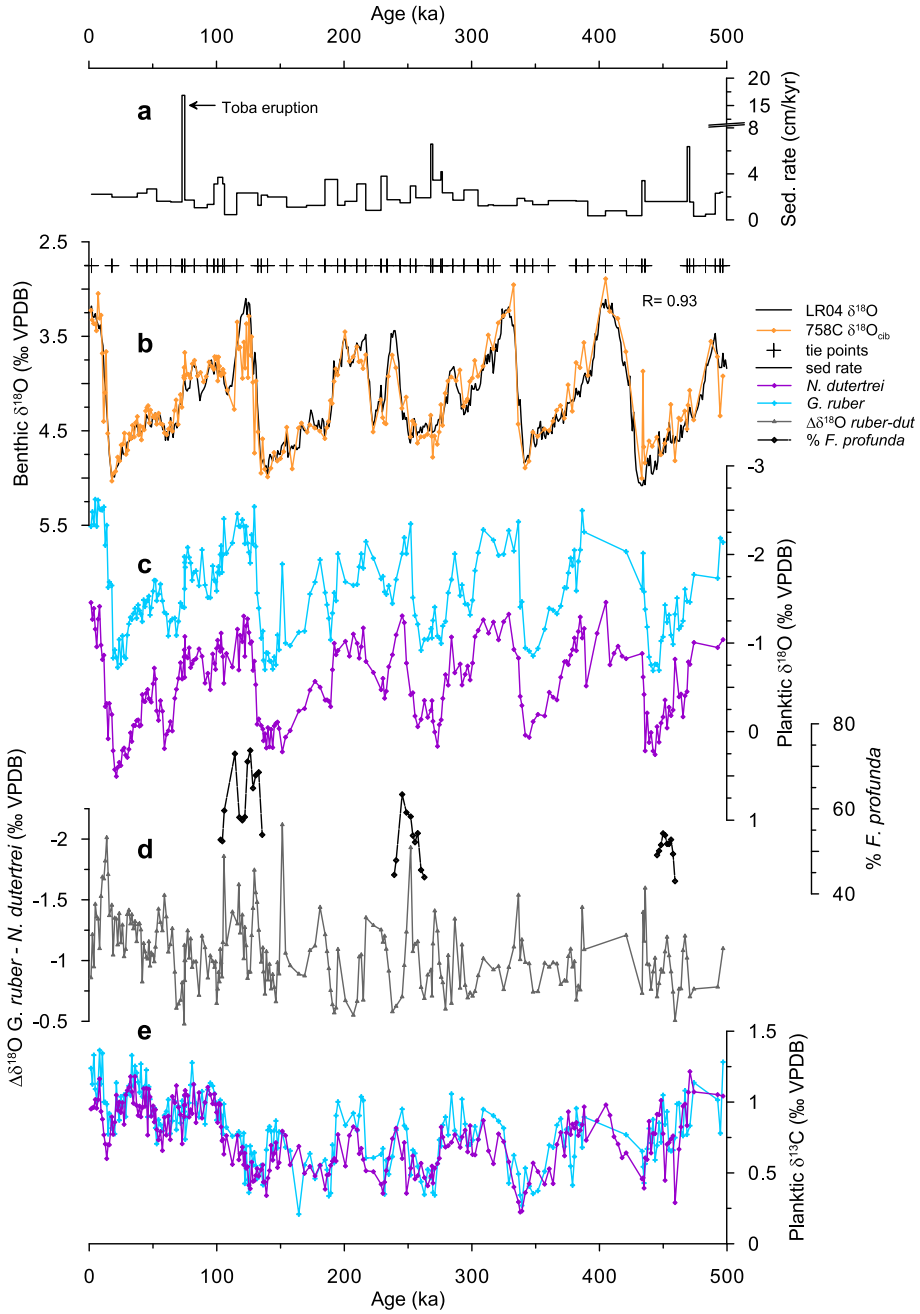

Fig. 2. ODP Hole 758C age model and palaeoclimate records. (a) Sedimentation rates and age tie points (crosses), (b) Site 758 *C. wuellerstorfi* $\delta^{18}O$ record (orange) and the LR04 benthic foraminiferal $\delta^{18}O$ stack (black, Lisiecki and Raymo, 2005), (c) Site 758 planktic $\delta^{18}O$ records: *G. ruber* (blue) and *N. dutertrei* (purple), (d) Site 758 $\Delta\delta^{18}O_{r-d}$ record (grey, maximum stratification plotted up) and percent *F. profunda* coccoliths (black, minimum productivity plotted up) and (e) Site 758 planktic $\delta^{13}C$ records: *G. ruber* (blue) and *N. dutertrei* (purple). (For interpretation of the references to colour in this figure legend, the reader is referred to the web version of this article.)

found in Site 758C sediments (~74.5 ka) agrees well with published estimates for the timing of this volcanic eruption (74 ± 2 ka; Oppenheimer, 2002). Our sampling strategy resulted in isotope records with a mean temporal resolution of ~1.3 ka during the last 150 ka and ~2.7 ka for the interval between 150 and 500 ka (Fig. 2).

As an additional proxy indicator of stratification via its effect on photic zone productivity (e.g. Molfino and McIntyre, 1990; Beaufort et al., 1997, 2001), *Florisphaera profunda* coccolith counts were performed over three $\Delta\delta^{18}O_{r-d}$ cycles distributed throughout the record. To determine the relative abundance of *F. profunda*, a lower photic zone dwelling coccolithophore species, counts versus all other species (mostly small placoliths) were made from standard smear slides. At least 600 coccoliths were counted from a minimum of 12 fields of view by light microscope under cross-polarized light at ×1500 magnification.

To identify statistically significant periodicities, spectral analyses on $\delta^{18}O$ and $\Delta\delta^{18}O_{r-d}$ records were performed with SSA-MTM Toolkit software (Ghil et al., 2002) using the multi-taper method assuming a red noise model. To quantify coherence and phase lags between records, cross-spectral analyses were carried out using ARAND software (Howell et al., 2006). Datasets were interpolated to constant mean age steps prior to spectral and cross-spectral analyses ($\Delta T = 2.01–2.23$ ka, depending on the record analysed). The $\Delta\delta^{18}O_{r-d}$ record was filtered to isolate significant frequencies of variance using specific filters, designed based on significant spectral peaks, using Analyseries (Paillard et al., 1996) (filter: frequency 0.045, bandwidth 0.008, to capture 19 and 23 ka peaks).

4. Results

At Site 758, *C. wuellerstorfi* $\delta^{18}O$ ($\delta^{18}O_{cib}$) records 1.75‰ glacial–interglacial (G–I) ~100 ka cycles, similar in magnitude to the LR04 stack (Fig. 2) but with slightly lighter values during some peak interglacials. *G. ruber* and *N. dutertrei* $\delta^{18}O$ ($\delta^{18}O_r$ and $\delta^{18}O_d$, respectively) record G–I oscillations similar in amplitude to *C. wuellerstorfi*, but with more variability at higher frequencies (Fig. 2b and c). $\delta^{13}C$ records for *G. ruber* and *N. dutertrei* have muted G–I variability compared to $\delta^{18}O$ records, with similar values and trends for both planktic species throughout the record (Fig. 2e). Spectral analyses of planktic and benthic $\delta^{18}O$ records indicate strong spectral power (>99% confidence) at the 100 ka, 41 ka, and 23 ka orbital periodicities (Fig. 3a–c). The $\delta^{18}O_d$ power spectrum closely resembles that of $\delta^{18}O_{cib}$, with strong power at all three main orbital periods, but contains slightly more power at the precession period than $\delta^{18}O_{cib}$. $\delta^{18}O_r$ contains strong spectral power in the precession band, and relatively less power at the longer orbital periods than the benthic and thermocline-dwelling species (Fig. 3a–c). Spectral analysis of the $\Delta\delta^{18}O_{r-d}$ record indicates significant variance (>99% confidence) at frequencies corresponding to 23, 19 and 11 ka (primary and harmonic of precession) (Fig. 3d). Analyses of individual portions of the $\Delta\delta^{18}O_{r-d}$ record (0–150 ka and 150–500 ka; not shown) indicate that a significant ~11 ka period is found only in the higher-resolution interval, which suggests that variability at this period may be aliased in the lower-resolution part of the record.

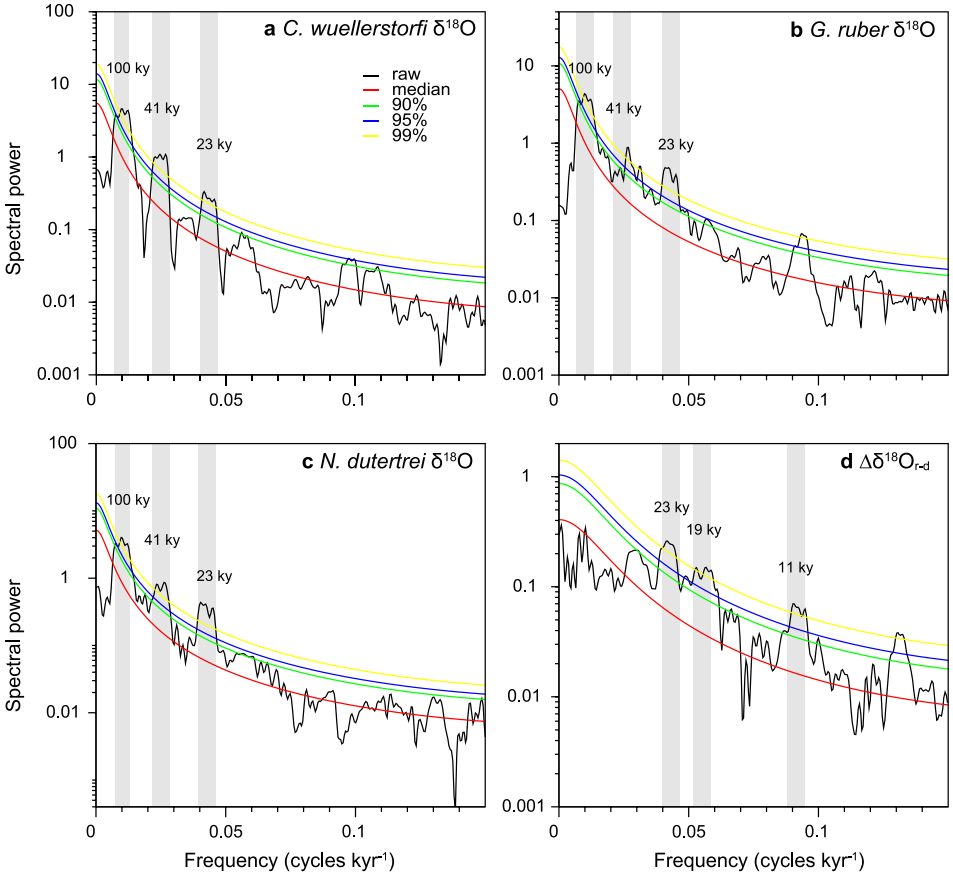

Fig. 3. Spectral power versus frequency plots for Site 758 $\delta^{18}O$ records. (a) *C. wuellerstorfi*, (b) *G. ruber*, (c) *N. dutertrei* and (d) $\Delta\delta^{18}O_{r-d}$. Significant orbital frequencies are highlighted.

Cross-spectral analyses indicate that both planktic $\delta^{18}O$ records are highly coherent with $\delta^{18}O_{cib}$ at the main orbital frequencies (>95% confidence level); however, the three records are not consistently in phase with each other (Table 1). Phase differences cannot be an age model artefact because all signals come from the same samples and, thus, are co-registered. At the 41-ka and 23-ka periods, $\delta^{18}O_d$ is in phase with $\delta^{18}O_{cib}$ (within error). While $\delta^{18}O_r$ is also in phase with $\delta^{18}O_{cib}$ at the 41-ka period, $\delta^{18}O_r$ leads $\delta^{18}O_{cib}$ by 3.9 ka at the 23-ka period (23 ka*61°/360° = 3.9 ka). This temporal lead of $\delta^{18}O_r$ over $\delta^{18}O_d$ and $\delta^{18}O_{cib}$ is visible with the naked eye at the major transitions (Fig. 2). $\Delta\delta^{18}O_{r-d}$ is coherent with $\delta^{18}O_{cib}$ at the 80% confidence level (41 ka) or 95% confidence level (23 ka). Highest values in $\Delta\delta^{18}O_{r-d}$ (i.e. minima in the $\delta^{18}O$ difference between *G. ruber* and *N. dutertrei*) lag lowest values in $\delta^{18}O_{cib}$ (ice volume minima) by $-48 \pm 40°$ (5.5 ± 4.6 ka) at the 41-ka period and by $-70 \pm 18°$ (4.5 ± 1.1 ka) at the 23-ka period (Table 1, Fig. 4).

We also ran cross-spectral analyses between the Hole 758C $\Delta\delta^{18}O_{r-d}$ record and other climate and monsoon proxy records: namely local insolation, two Arabian Sea summer monsoon stacked records (Clemens and Prell, 2003; Caley et al., 2011b), and a composite Chinese cave speleothem $\delta^{18}O$ record (Cheng et al., 2009) (Table 1). We find that $\Delta\delta^{18}O_{r-d}$ is not significantly coherent with local absolute maximum insolation (computed using the code of Huybers (2006) for 5°N, see discussion). However, visually, maxima in local insolation (P min) and $\Delta\delta^{18}O_{r-d}$ minima are sometimes aligned and where this is not the case, a lead of $\Delta\delta^{18}O_{r-d}$ (min.) over insolation (max.) in both raw and filtered (19–23 ka component) records can be seen (Fig. 5). Coherence of $\Delta\delta^{18}O_{r-d}$ with the Caley et al. (2011b) ISM stack at the precession band is high (>95% confidence level) and maximum $\Delta\delta^{18}O_{r-d}$ is in phase with maximum ISM intensity (10 ± 27°). Coherence between $\Delta\delta^{18}O_{r-d}$ and the Clemens and Prell (2003) summer monsoon stack at the precession band is lower (>80% confidence level) and a similar in-phase relationship is found between maximum $\Delta\delta^{18}O_{r-d}$ and maximum summer monsoon intensity ($-10 \pm 27°$). At the precession band, coherence between $\Delta\delta^{18}O_{r-d}$ and Chinese cave $\delta^{18}O$ is high (>95% confidence level) and maximum $\Delta\delta^{18}O_{r-d}$ lags minimum cave $\delta^{18}O$ by 88 ± 19° (5.7 ± 1.2 ka).

During the three $\Delta\delta^{18}O_{r-d}$ ~23 ka cycles in which *F. profunda* coccoliths were counted, higher relative abundances are consistently associated with $\Delta\delta^{18}O_{r-d}$ minima (Fig. 2d). Relative abundances of *F. profunda* range from 73% to 43%, and appear to be scaled to the magnitude of concurrent $\Delta\delta^{18}O_{r-d}$ changes (Fig. 2d).

5. Discussion

5.1. Depth habitats and interpretation of $\Delta\delta^{18}O_{r-d}$

Application of $\Delta\delta^{18}O$ to reconstruction of upper water column structure is dependent on the differential depth habitats of the studied foraminiferal species. *G. ruber* (white) is thought to live and calcify in the upper mixed layer (<60 m depth) of the ocean (Fairbanks et al., 1980, 1982; Hemleben et al., 1989), with individuals of *G. ruber sensu stricto* (*s.s.*) living at shallower depths (<30 m) relative to the *sensu lato* morphotype (30–60 m) (Wang, 2000). *N. dutertrei* is generally most abundant at the thermocline (60–150 m) (Fairbanks et al., 1982; Curry et al., 1983). A recent study of equatorial Indian Ocean surface sediments confirms similar depth habitat estimates in our study region, with *G. ruber s.s.* living at 20–50 m and *N. dutertrei* at 75–100 m in the upper thermocline (Mohtadi et al., 2011). However, the assumption that the depth habitat of a given species in the past remained constant and similar to that observed in the modern ocean is not always accurate (e.g. Field, 2004; Rohling et al., 2004). *G. ruber* (white) appears to maintain a near-surface depth habitat despite significant freshwater inputs in other regions (Schmuker and Schiebel, 2002; Rohling et al., 2004). In temperate waters offshore of California, with a much wider range of seasonal oceanographic variability compared to Site 758, *G. ruber* was found to have only a small-scale response to deepening isotherms and *N. dutertrei* abundance covaried with the depth of a given isotherm within the thermocline (Field, 2004). A significant seasonal migration or calcification bias in either species in response to SST or SSS change is unlikely given the small intra-annual ranges of these parameters in our tropical study area (Section 2). Similarly, seasonal primary productivity changes (i.e. potential food availability fluctuations) are small

Table 1
Coherence and phase relationships relative to $\delta^{18}O_{benthic}$[a], Site 758 $\delta^{18}O_{r-d}$ and orbital parameters.

Proxy record	$\delta^{18}O$-41 ka		Obliquity phase	$\delta^{18}O$-23 ka		Precession phase[d]
	Coherency[b]	Phase(°)[c]	Phase[d]	Coherency[b]	Phase(°)[c]	
Coherence and phase relative to site-specific $\delta^{18}O_{benthic}$[a]						
758 *G. ruber* $\delta^{18}O$	0.82	+24° (±25)	−37°	0.87	+61° (±20)	−11°
758 *N. dutertrei* $\delta^{18}O$	0.87	+8° (±20)	−53°	0.80	+16° (±26)	−56°
758 $\Delta\delta^{18}O_{r-d}$[e]	0.61	−48° (±40)	−109°	0.90	−70° (±18)	−142°
Arabian Sea						
Clemens and Prell (2003) SM stack	0.84	+57° (±28)	−4°	0.96	−43° (±14)	−115°
Clemens and Prell (2003) SM factor	0.86	+63° (±18)	+2°	0.97	−47° (±8)	−119°
WM maxima (Clemens et al., 2008, 0–1.25 Ma)			−286° (±35)			−298° (±9)
Caley et al. (2011) SM stack (non-orbital age model)			−53° (±20)			−141° (±15)

Proxy record	$\delta^{18}O$-41 ka		$\delta^{18}O$-23 ka	
	Coherency[f]	Phase(°)[g]	Coherency[f]	Phase(°)[g]
Coherence and phase relative to site 758 $\delta^{18}O_{r-d}$[e]				
Clemens and Prell (2003) SM stack	0.86	−100° (±14)	0.65	−10° (±27)
Caley et al. (2011b) SM stack (non-orbital age model)	0.68	−40° (±36)	0.80	+10° (±27)
Chinese cave speleothem $\delta^{18}O$ (Cheng et al., 2009)	0.82	+97° (±17)	0.78	+88° (±19)

[a] $\delta^{18}O_{benthic}$ multiplied by −1 so that higher values correspond to ice minima.
[b] Test statistic for non-zero coherency at the 80% and 95% level are 0.60 and 0.75 respectively.
[c] Negative phase indicates a lag of the proxy record relative to $\delta^{18}O_{benthic}$ and positive phase indicates a lead.
[d] Calculated by applying the LR04-calculated phase lags of −61° and −72° for obliquity and precession respectively.
[e] $\Delta\delta^{18}O_{r-d}$ NOT multiplied by −1, thus higher values correspond to stratification minima.
[f] Test statistic for non-zero coherency at the 80% and 95% level are 0.63 and 0.78 respectively.
[g] Negative phase indicates a lag of the proxy record relative to 758 $\delta^{18}O_{r-d}$ and positive phase indicates a lead.

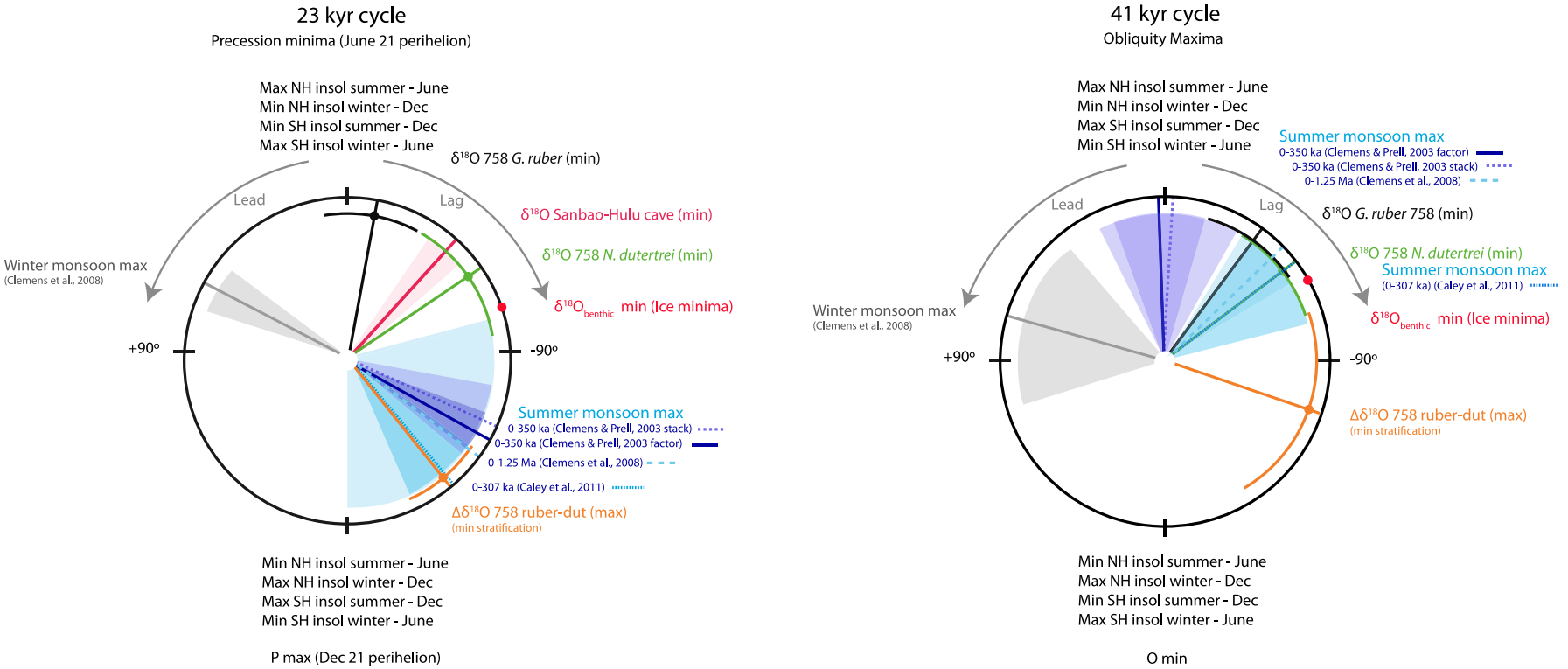

Fig. 4. Phase wheels summarizing the late Pleistocene monsoon response to insolation forcing at the orbital precession (23 ka) and obliquity (41 ka) periods. The precession index is defined as $\Delta e \sin\omega$ where ω is the longitude of the perihelion measured from the moving vernal point and e is the eccentricity of Earth's orbit about the Sun (Berger and Loutre, 1977; Laskar et al., 1993). Obliquity is the tilt of Earth's axis with respect to the ecliptic plane. Zero phase is set to precession minima (P min; $\omega = 90°$, 21st June perihelion) and obliquity maxima (O max), respectively. Negative phases are measured in the clockwise direction and represent phase lags relative to P min or O max. Positive phases are measured in the anticlockwise direction and represent phase leads relative to P min or O max. Phase relationships of ice volume are also shown (red dots, Lisiecki and Raymo, 2005). All Site 758 isotope records are coherent with Site 758 $\delta^{18}O_{benthic}$ at the 95% confidence level except $\Delta\delta^{18}O_{r-d}$ at the obliquity period (80% confidence level) (Table 1). Published records plotted (with shaded phase estimate errors) are the Arabian Sea summer monsoon stack (Caley et al., 2011b), the Arabian Sea summer monsoon stack and summer monsoon factor (Clemens and Prell, 2003), the Chinese Sanbao-Hulu composite cave $\delta^{18}O$ (Cheng et al., 2009), and winter and summer monsoon maxima (Clemens et al., 2008). NH = northern hemisphere, SH = southern hemisphere. (For interpretation of the references to colour in this figure legend, the reader is referred to the web version of this article.)

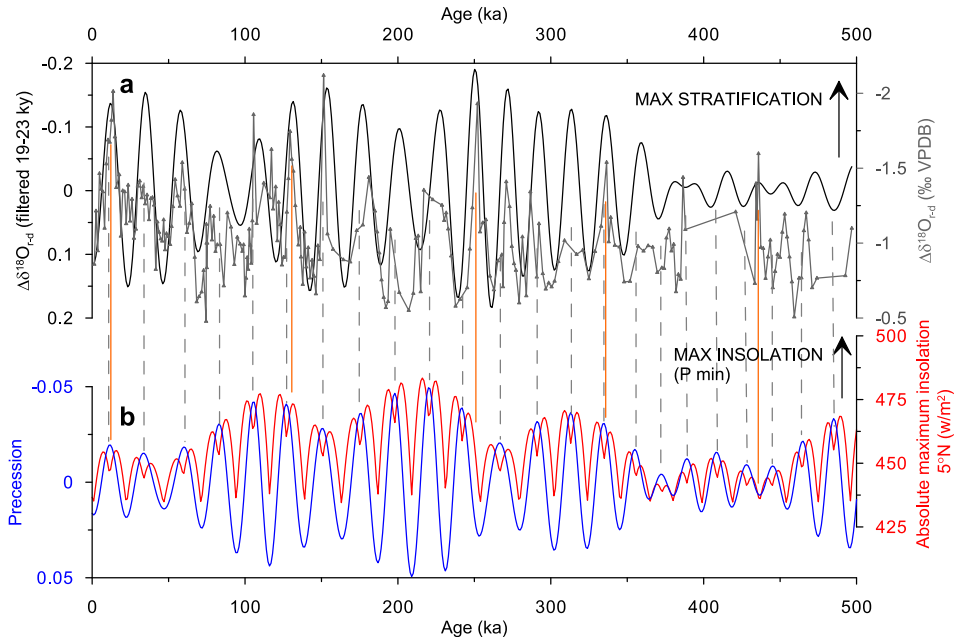

Fig. 5. Site 758 stratification compared to insolation forcing. (a) Site 758 $\Delta\delta^{18}O_{r-d}$ record (maximum stratification plotted up), raw (grey) and filtered to illustrate only variance at the 19 and 23 ka precession periods (black; filter: frequency 0.045, bandwidth 0.008). (b) Precession (blue) and absolute maximum insolation at 5°N (red) (Huybers, 2006). Grey dotted lines illustrate P minima, solid orange lines indicate the five stratification peaks that occur at the onset of glacial terminations. (For interpretation of the references to colour in this figure legend, the reader is referred to the web version of this article.)

(http://seawifs.gsfc.nasa.gov/SEAWIFS.html). By looking at a single open-ocean 'warm pool' site, we minimise any potential spatial and circulation-driven variations in $\Delta\delta^{18}O$ (e.g. Steph et al., 2009). Thus, we infer that orbital timescale variance in $\Delta\delta^{18}O_{r-d}$ at Site 758 during the Pleistocene is not primarily governed by changing foraminiferal depth habitat and is unlikely to be significantly seasonally biased.

Changes in the $\delta^{18}O$ difference between shallow and deeper-dwelling planktic foraminiferal species, denoted here as $\Delta\delta^{18}O_{r-d}$, are classically interpreted in terms of thermocline depth changes. In the tropics, thermocline depth is controlled by physical processes such as the depth of wind-driven mixing, upwelling strength, and the intensity of solar radiation related to season and orbital configuration. Thus, a large $\Delta\delta^{18}O$ suggests a shallow thermocline and strong vertical temperature gradients (ΔT) in the photic zone, while a small $\Delta\delta^{18}O$ implies a deep thermocline with relatively weak ΔT (Ravelo and Shackleton, 1995; Steinke et al., 2010; Steph et al., 2009, 2010). Salinity gradients in the surface ocean, generated by precipitation-evaporation changes on seasonal to orbital timescales, also strongly affect $\Delta\delta^{18}O$ in some regions (e.g. Rohling et al., 2004; Mohtadi et al., 2009; Steinke et al., 2010).

Several factors suggest that the Site 758 $\Delta\delta^{18}O_{r-d}$ signal is primarily driven by *G. ruber* (surface ocean variability) rather than *N. dutertrei* (intermediate water variability). First, when the global sea-level component of both planktic $\delta^{18}O$ records is removed, residual variations in $\delta^{18}O_r$ have greater amplitude ($1\sigma = 0.33‰$) than those of $\delta^{18}O_d$ ($1\sigma = 0.25‰$) (Fig. 6). Second, the similar spectral power profile and phasing of $\delta^{18}O_d$ to $\delta^{18}O_{cib}$ suggests that *N. dutertrei* is primarily responding to the global adjustment to ice-volume changes rather than to local forcing (Fig. 3). This is consistent with the finding that *G. ruber* leads both deeper-dwelling species in the precession band and that all significant periods of variance in $\Delta\delta^{18}O_{r-d}$ are precession related – a reflection of the dominant 'top–down' orbital control on tropical climate (e.g. Clement et al., 2004). Thus, $\Delta\delta^{18}O_{r-d}$ maxima (i.e. more positive values, which represent minima in the $\delta^{18}O$ difference between the two species) in our record could be driven by some combination of (1) a decrease in direct insolation forcing, (2) an increase in the depth of wind-driven mixing during times of greater wind strengths, and (3) decreased surface freshening through direct input or runoff of monsoonal precipitation and increased evaporation rates during times with greater wind strengths. All of these factors would result in weakening of vertical stratification in the upper water column.

A significant influence on $\Delta\delta^{18}O_{r-d}$ from monsoon-related changes in SSS is unlikely, given that Site 758 is located on or near the 34 psu isohaline all year round and is relatively unaffected by large seasonal freshwater inputs in the northern BOB (Antonov et al., 2010, Fig. 1e and f). On the other hand, surface wind strength at Site 758 is twice as high during summer compared to winter (Fig. 1). We, therefore, interpret $\Delta\delta^{18}O_{r-d}$ at Site 758 as reflecting, to some degree, variations in stratification controlled by the depth of wind-driven mixing along with variations in wind-driven evaporation. Strengthened winds then caused stronger mixing and increased evaporation, both of which act to reduce vertical stratification. Some influence of direct insolation forcing on $\Delta\delta^{18}O_{r-d}$ is also likely, given that SST reconstructions indicate greater SST variability on orbital timescales in the region of Site 758 compared to that over the seasonal cycle. Planktic foraminifera-based transfer functions suggest warm-season SSTs in the range ~26–30 °C and cold-season SSTs in the range ~23–30 °C over the last 500 ka at Site 758, although application of this proxy may have been compromised by poor foraminiferal preservation in some intervals, leading to underestimation of SSTs (Chen, 1994). Paired $\delta^{18}O$–Mg/Ca analyses on *G. ruber* in two cores from the northern BOB and the Andaman Sea suggest that Last Glacial SSTs were ~3 °C lower than modern in this region (Rachid et al., 2007, 2011). Assuming a 0.2‰ $\delta^{18}O$ change per °C (Kim and O'Neil, 1997), 3 °C SST changes on G-I timescales could account for around half of the amplitude of residual variability in $\delta^{18}O_r$ at Site 758 (Fig. 6b). Our interpretation of $\Delta\delta^{18}O_{r-d}$ described above is consistent with *F. profunda* abundance data that indicate maximum stratification (minimum upper photic zone productivity) at times of minimum $\Delta\delta^{18}O_{r-d}$ (Fig. 2), as well as

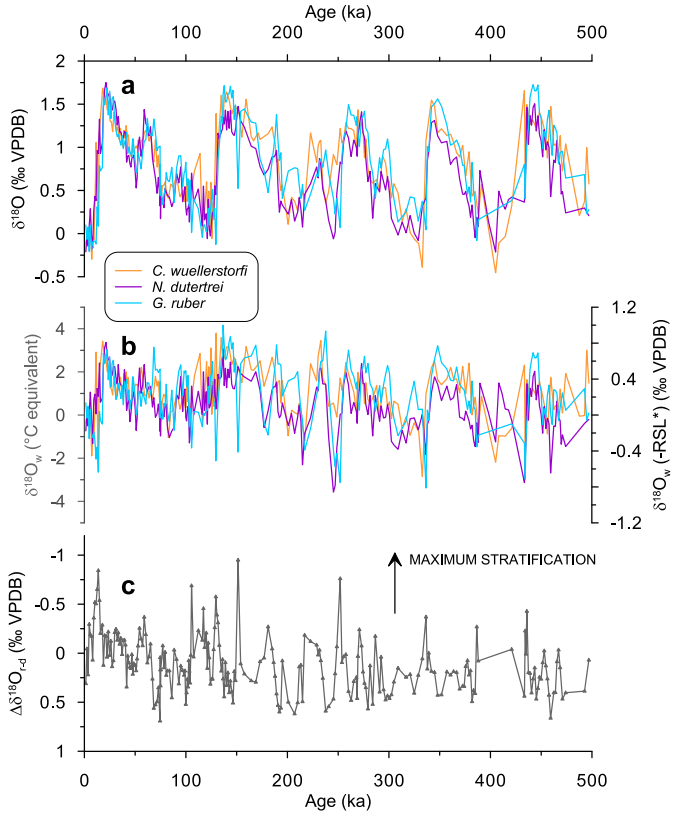

Fig. 6. $\delta^{18}O$ records for Site 758. (a) Site 758 $\delta^{18}O$ records for the three foraminiferal species (colours as in Fig. 2). (b) Site 758 $\delta^{18}O$ records for the three foraminiferal species minus variance attributed to global sea level change. The sea level component was removed by subtracting the Red Sea relative sea level curve of Rohling et al. (2009a, 2010) rescaled to the age scales of the Site 758 records, from foraminiferal $\delta^{18}O$ assuming a 0.01‰ change in $\delta^{18}O$ per metre of sea level change (Adkins and Schrag, 2001). The local temperature component was not subtracted because no sea surface temperature (SST) record exists for our site; therefore, the resultant $\delta^{18}O_w$ records include local SST and salinity components. (c) Site 758 $\Delta\delta^{18}O_{r-d}$ record (maximum stratification plotted up). All data are normalised to mean values for 0–6 ka and plotted with positive values up except $\Delta\delta^{18}O_{r-d}$, which has an inverted axis so that maximum stratification points up.

with orbital phase relationships between $\Delta\delta^{18}O_{r-d}$ and other records, as discussed in section 5.3.

5.2. Planktic foraminiferal carbon isotope data and productivity

The absence of a $\delta^{13}C$ gradient between *G. ruber* and *N. dutertrei* (<0.2‰, Fig. 2e) throughout the study interval at Site 758 at first appears at odds with fluctuations in *F. profunda* abundance at Site 758 (Fig. 2d). The relative abundance of *F. profunda* has been calibrated to changes in Indian Ocean primary productivity, and relatively low but variable values (~100–160 gC m^{-2} yr^{-1}) can be inferred from *F. profunda* abundances of 43–73% at Site 758 (Beaufort et al., 1997, 2001). Because of biological activity in the upper ocean, *G. ruber* might be expected to record the more positive $\delta^{13}C$ signature of the dissolved inorganic carbon pool ($\delta^{13}C_{DIC}$) in the upper photic zone due to preferential uptake of isotopically light CO_2 by photosynthesizing organisms, whereas *N. dutertrei* might record a more negative $\delta^{13}C_{DIC}$ due to remineralisation of ^{12}C-rich organic matter at depth and nutrient inputs into the thermocline (Kroopnick, 1974). However, as well as being affected by $\delta^{13}C_{DIC}$ during equilibrium fractionation, foraminiferal shell $\delta^{13}C$ is influenced by environmental factors such as carbonate ion concentration, pH and temperature (Spero et al., 1997; Bijma et al., 1999; Bemis et al., 2000) and physiological factors like foraminiferal respiration and symbiont photosynthesis (both *G. ruber* and *N. dutertrei* are symbiont-bearing) (Spero and Lea, 1996; Bemis et al., 2000). This complicates interpretation of foraminiferal shell $\delta^{13}C$ purely in terms of productivity. For example, in the eastern equatorial Pacific Ocean, a region with high productivity and strong physicochemical gradients in the upper water column, a number of records do not contain the expected $\delta^{13}C$ gradients between *G. ruber* and *N. dutertrei* (Spero et al., 2003; Pena et al., 2008; Leduc et al., 2010). Spero et al. (2003) proposed species-specific normalisation factors, derived from experimental and plankton tow studies, to correct foraminiferal $\delta^{13}C$ to $\delta^{13}C_{DIC}$. Application of these normalisation corrections to our records (+0.94‰ for *G. ruber* and −0.50‰ for *N. dutertrei*) would restore the expected $\delta^{13}C$ gradient between these upper photic zone and thermocline species at Site 758, however local modern offsets between foraminifera and DIC in the region of Site 758 would first need to be constrained.

5.3. Precession-band phases of Site 758 $\Delta\delta^{18}O_{r-d}$ relative to climate and monsoon records

To elucidate potential forcing mechanisms on Site 758 stratification, which is dominated by variance at precession and half-precession frequencies, we first compare $\Delta\delta^{18}O_{r-d}$ with absolute maximum annual insolation (Fig. 5). Following Huybers (2006), maximum integrated summer insolation values are extracted from a matrix of daily isolation values at 5°N, thereby incorporating all past orbital configurations at a given latitude and time without artificially tying to a prescribed orbital configuration. For example, the commonly used 21st July insolation curve is derived assuming that ω, the longitude of the perihelion measured from the moving vernal point, equals 120° (Berger, 1978; Berger et al., 1993). Although Site 758 $\Delta\delta^{18}O_{r-d}$ is not significantly coherent with absolute maximum insolation, visual comparison of the two records indicates that peaks in Site 758 stratification sometimes coincide with insolation maxima (P minima, dashed lines in Fig. 5), which suggests a component of direct insolation forcing.

The 11 ka period identified in the Site 758 stratification record (Fig. 3) may also originate from insolation variations. On the equator, the sun passes overhead twice a year. The resultant double maximum in annual insolation can generate a half-precession (~11 ka) signal in tropical insolation forcing, the amplitude of which decreases rapidly away from the equator (Berger and Loutre, 1997; Berger et al., 2006). At 5°N, the 11-ka insolation component is still relatively strong (Fig. 5b). Modulation of monsoon dynamics by equatorial insolation as suggested by the presence of a semi-precession signal has been inferred for a number of other palaeo-records, for example, Chinese Loess Asian summer monsoon records (Sun and Huang, 2006), foraminiferal $\Delta\delta^{13}C$ from the South China Sea (Wang et al., 2003b) and African monsoon rainfall patterns (Verschuren et al., 2009). An alternative monsoon-related means of generating an ~11 ka signal in $\Delta\delta^{18}O_{r-d}$ is via the combined forcing of maximum monsoon rainfall near P maxima and maximum insolation heating at P minima. This scenario, however, is less likely given the minimal influence of monsoon-related freshwater input at Site 758. An influence of other forcing mechanism(s), in addition to insolation, on Site 758 $\Delta\delta^{18}O_{r-d}$ is implied by the ~9 ka lag (~2.4 ka lead) of minimum (maximum) stratification relative to northern hemisphere (NH) summer insolation maxima (P min) when the precession phase is averaged over the entire record (Fig. 4, Table 1).

Over the past ~350 ka (where records overlap), stratification minima at Site 758 are in phase with ISM maxima inferred from two independent stacked proxy records from the Arabian Sea (Figs. 4 and 7). The Clemens and Prell (2003) summer monsoon

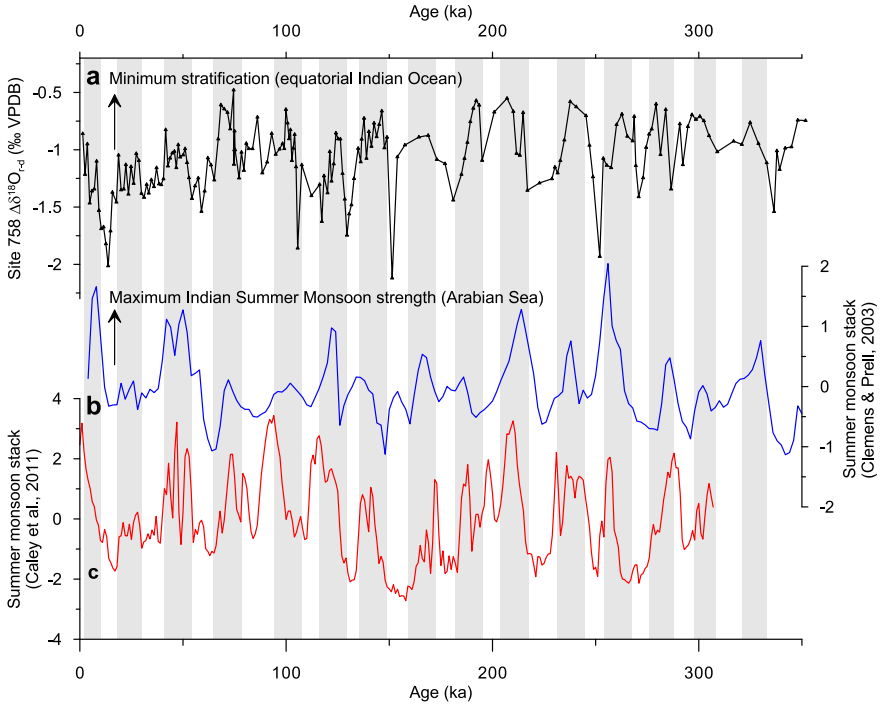

Fig. 7. Comparison of the Site 758 stratification record with two Arabian Sea summer monsoon stacks. (a) Site 758 $\Delta\delta^{18}O_{r-d}$ record (minimum stratification plotted up), (b) Arabian Sea summer monsoon stack (Clemens and Prell, 2003), and (c) Arabian Sea summer monsoon stack (Caley et al., 2011b).

stack, which consists of five distinct palaeoproductivity and lithogenic grain-size records on an orbitally-tuned age model, is interpreted as reflecting ISM strength via wind and upwelling intensity and lags maximum NH summer insolation (P min) by ~8 ka in the precession band. The Caley et al. (2011b) stack, which comprises three independent ISM proxies from an Arabian Sea sediment core on an age model independent of orbital tuning, has a similar ~9 ka lag between inferred maximum ISM strength and maximum NH summer insolation in the precession band. The in-phase relationship between Site 758 stratification minima and inferred Arabian Sea ISM strength maxima is consistent with a common ISM wind forcing in the Arabian Sea and the eastern equatorial Indian Ocean, which would increase the depth of mixing and reduce stratification at Site 758, while intensifying upwelling and aeolian particle delivery to the Arabian Sea. Our new stratification record provides remote support for the 8–9 ka precession band phase lag observed previously between NH summer insolation maxima and ISM strength maxima in the Arabian Sea and other regions (Clemens et al., 1991, 2008; Altabet et al., 1995; Morley and Heusser, 1997; Reichart et al., 1998; Chen et al., 2003; Clemens and Prell, 2003; Caley et al., 2011b). The high coherency and in-phase relationship between Site 758 and both Arabian Sea records (Table 1) supports the original interpretation that ISM strength provides the dominant forcing on Arabian Sea palaeoproductivity, which has recently been called into question by the suggestion that circulation changes and ensuing nutrient delivery exerted a primary control on these records (Ziegler et al., 2010). This large lag indicates that ISM wind strength maxima at the precession band are not directly forced by changes in NH summer insolation; other mechanisms must also be involved.

Site 758 $\Delta\delta^{18}O_{r-d}$ is highly coherent with a cave speleothem composite $\delta^{18}O$ record from southeast China (Cheng et al., 2009); however, the two records differ in their precession band phases by approximately 5 ka. Minimum stratification lags maximum NH summer insolation (P min) by 142° or ~9 ka, whereas light cave $\delta^{18}O$ lags P min by 45° or ~2.9 ka. This interpretation and orbital phasing of Chinese cave $\delta^{18}O$ palaeo-monsoon records have previously been considered in detail (e.g. Clemens et al., 2010; Pausata et al., 2011). These authors suggested that the Chinese cave $\delta^{18}O$ records, which are typically interpreted as recording solely summer monsoon rainfall strength, reflect an integrated signal of summer monsoon circulation as recorded in the Arabian Sea and the effect of winter temperatures on the local $\delta^{18}O$ signature of precipitation. On the basis of a 90° phase difference in the precession band, it is unlikely that the Site 758 stratification record and the cave $\delta^{18}O$ record share a common direct driving mechanism. If stratification minima at Site 758 record the timing of strong ISM winds, the long (~9 ka) phase lag between maximum NH insolation (P min) and stratification minima likely reflects multiple forcing mechanisms; namely insolation, ice volume and latent heat export from the SSIO (Clemens and Prell, 2003; Clemens et al., 2008, 2010; Caley et al., 2011b). However, we cannot yet rule out the possibility that the different phase response of cave $\delta^{18}O$ in southeast China and ISM wind strength in the Indian Ocean reflects a decoupling of monsoon wind strength and precipitation.

5.4. Millennial-scale events and teleconnections

Five of the largest stratification peaks at Site 758 as recorded by $\Delta\delta^{18}O_{r-d}$ occur at the onset of glacial terminations (Figs. 2, 5 and 8). We suggest that these may be manifestations of remote millennial-scale climate events. Site 758 stratification is compared with a high-resolution Red Sea atmospheric dust record (Roberts et al., 2011) and a North Atlantic record of ice-rafting ('Heinrich') events from IODP Site 1308 (Hodell et al., 2008) in Fig. 8. While the Red Sea dust record is on an independent U–Th validated chronology (Rohling et al., 2009a, 2010), the Site 1308 and 758 records are tuned to the LR04 benthic $\delta^{18}O$ stack (Lisiecki and Raymo, 2005), which results in some offsets between records. Taking into account discrepancies in the exact timing of terminations in the LR04 versus Red Sea chronologies (Fig. 8a) and differences between the Site 758 and 1308 LR04-tuned chronologies (Fig. 8b), stratification maxima

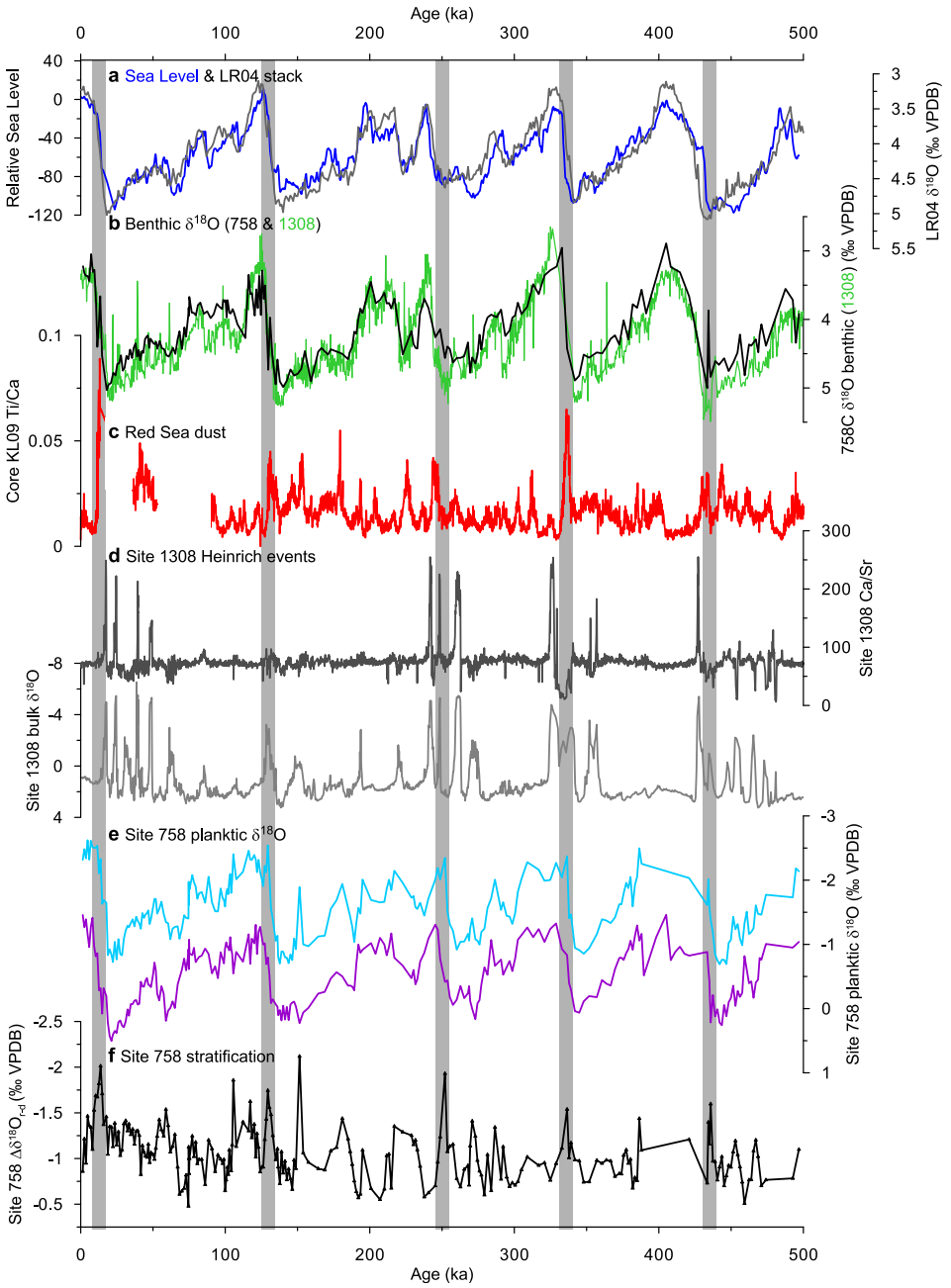

Fig. 8. Correlation of terminal stratification peaks at Site 758 with remote millennial-scale climate events. (a) Red Sea relative sea level record, 1 ka Gaussian smoothing applied (blue; Rohling et al., 2009a,b, 2010) and the LR04 benthic foraminiferal $\delta^{18}O$ stack (black; Lisiecki and Raymo, 2005), (b) benthic foraminiferal $\delta^{18}O$ records for Site 758 (black; this study) and Site 1308 (green; Hodell et al., 2008), (c) Red Sea dust proxy record (Ti/Ca), 1 ka Gaussian smoothing applied (Roberts et al., 2011), (d) IODP Site 1308 North Atlantic ice-rafted debris proxy records, Ca/Sr ratios and bulk sediment $\delta^{18}O$ (Hodell et al., 2008), (e) Site 758 planktic foraminiferal $\delta^{18}O$ records and (f) Site 758 $\Delta\delta^{18}O_{r-d}$ record (maximum stratification plotted up). Grey bands highlight stratification peaks at glacial terminations. (For interpretation of the references to colour in this figure legend, the reader is referred to the web version of this article.)

at terminations broadly coincide with large dust peaks and North Atlantic 'terminal' Heinrich events. Major dust maxima in the early stages of terminations have been identified in high-resolution records from both the Red Sea (Roberts et al., 2011) and the Chinese Loess (Sun et al., 2006). Although higher-resolution records at Site 758 and a common chronology are required to document precise relative timings, correlation between cold North Atlantic Heinrich events, enhanced dust flux, and strong Indian Ocean stratification (implying weak summer monsoon winds) is consistent with models that simulate stronger westerly winds over Eurasia and weaker summer monsoons during Heinrich events (Jin et al., 2007). A link between abrupt North Atlantic cold events and weak Asian summer monsoons has been inferred from summer monsoon proxy records in the Arabian Sea (Schulz et al., 1998; Gupta et al., 2003), Chinese Loess (Porter and An, 1995; An, 2000) and Chinese and Indian Ocean stalagmite $\delta^{18}O$ records (Wang et al., 2001; Burns et al., 2003, 2004; Cheng et al., 2006, 2009; Zhou et al., 2008). These links imply large-scale atmospheric teleconnections on millennial timescales (e.g. Rohling et al., 2003; Goswami et al., 2006; Pausata et al., 2011; Roberts et al., 2011). Strong equatorial Indian Ocean stratification during the early stages of terminations is consistent with a significant southern hemisphere control on millennial-scale

monsoon variability during glacial periods (Rohling et al., 2009b; An et al., 2011), potentially via modulation of the strength of the SSIO-Asia pressure gradient (An et al., 2011; Caley et al., 2013).

6. Conclusions

We present a new record of planktic foraminiferal $\Delta\delta^{18}O$ from eastern equatorial Indian Ocean ODP Site 758C spanning the last 500 ka, which we interpret as predominantly reflecting changes in ISM wind strength via its effect on stratification. The documented mean 9 ka lag between maximum NH insolation (P min) and minimum stratification (maximum ISM) in the precession band is similar to published phases of other ISM proxy records, principally from the Arabian Sea but also the South China Sea and Asian subcontinent. This suggests a common wind forcing between distinct ISM-influenced regions and supports the contention that the precession phasing of the ISM is driven by a combination of NH insolation, ice volume and latent heat export from the SSIO (Clemens et al., 2008, 2010). Significant variations in stratification at Site 758 occur at precession and half-precession frequencies (23, 19 and 11 ka), which suggests a component of local insolation forcing. Superimposed on orbital timescale variations, large stratification events during the early stages of terminations 1 to 5 are also evident in the Site 758 record. These strong stratification events appear to be temporally correlated with peaks in Arabian-Asian atmospheric dust and large North Atlantic Heinrich events, which is consistent with previously documented links between weak summer monsoon intervals and cold climate events in the North Atlantic.

Acknowledgements

This study was funded by the Japan Society for the Promotion of Science Invitational Program for Advanced Japanese Research Institutes and was supported by the Benedum Stable Isotope facility at Brown University. This work contributes to Australian Laureate Fellowship FL120100050. We are grateful to the members of JAMSTEC and the Centre for Advanced Marine Core Research (Kochi University) who assisted with this work, in particular Chisa Nishimori, Michiyo Kobayashi and Hirofumi Asahi.

References

Adkins, J.F., Schrag, D.P., 2001. Pore fluid constraints on deep ocean temperature and salinity during the Last Glacial Maximum. Geophysical Research Letters 28 (5), 771–774.

Altabet, M.A., Francois, R., Murray, D.W., Prell, W.L., 1995. Climate-related variations in denitrification in the Arabian Sea from sediment $^{15}N/^{14}N$ ratios. Nature 373, 506–509.

Altabet, M., Murray, D., Prell, W., 1999. Climatically linked oscillations in Arabian Sea denitrification over the last 1 m.y.: implications for marine N cycle. Paleoceanography 14, 732–743.

An, Z., 2000. The history and variability of the East Asian paleomonsoon climate. Quaternary Science Reviews 19, 171–187.

An, Z., Clemens, S.C., Shen, J., Qiang, X., Jin, Z., Sun, Y., Prell, W.L., Luo, J., Wang, S., Xu, H., Cai, Y., Zhou, W., Liu, X., Liu, W., Shi, Z., Yan, L., Xiao, X., Chang, H., Wu, F., Ai, L., Lu, F., 2011. Glacial–interglacial Indian summer monsoon dynamics. Science 333, 719–723.

Antonov, J.I., Seidov, D., Boyer, T.P., Locarnini, R.A., Mishonov, A.V., Garcia, H.E., Baranova, O.K., Zweng, M.M., Johnson, D.R., 2010. World Ocean Atlas 2009. In: Salinity, vol. 2. U.S. Government Printing Office, Washington, D.C., p. 184. NOAA Atlas NESDIS 69.

Aurahs, R., Treis, Y., Darling, K., Kucera, M., 2011. A revised taxonomic and phylogenetic concept for the planktonic foraminifer species *Globigerinoides ruber* based on molecular and morphometric evidence. Marine Micropaleontology 79, 1–14.

Bassinot, F.C., Marzin, C., Braconnot, P., Marti, O., Mathien-Blard, E., Lombard, F., Bopp, L., 2011. Holocene evolution of summer winds and marine productivity in the tropical Indian Ocean in response to insolation forcing: data-model comparison. Climate of the Past 7, 815–829.

Beaufort, L., Lancelot, Y., Camberlin, P., Cayre, O., Vincent, E., Bassinot, F., Labeyrie, L., 1997. Insolation cycles as a major control of equatorial Indian Ocean primary production. Science 278, 1451–1454.

Beaufort, L., de Garidel-Thoron, T., Mix, A.C., Pisias, N.G., 2001. ENSO-like forcing on oceanic primary production during the late Pleistocene. Science 293, 2440–2444.

Bemis, B., Spero, H.J., Lea, D.W., Bijma, J., 2000. Temperature influence on the carbon isotopic composition of *Orbulina universa* and *Globigerina bulloides* (planktic foraminifera). Marine Micropaleontology 38, 213–228.

Berger, A.L., 1978. Long-term variations of daily insolation and Quaternary climatic change. Journal of Atmospheric Science 35, 2362–2367.

Berger, A., Loutre, M.F., Tricot, C., 1993. Insolation and earth's orbital periods. Journal of Geophysical Research 98 (D6), 10341–10362.

Berger, A., Loutre, M.F., 1997. Inter tropical latitudes and precessional and half-precessional cycles. Science 278 (5342), 1476–1478.

Berger, A., Loutre, M.F., Mélice, J.-L., 2006. Equatorial insolation: from precession harmonics to eccentricity frequencies. Climate of the Past 2, 131–136.

Bijma, J., Spero, H., Lea, D., 1999. Reassessing foraminiferal stable isotope geochemistry: impact of the oceanic carbonate system (experimental results). In: Use of Proxies in Paleoceanography. Springer, Berlin Heidelberg, pp. 489–512.

Burns, S.J., Fleitmann, D., Matter, A., Kramers, J., Al-Subbary, A.A., 2003. Indian Ocean climate and an absolute chronology over Dansgaard/Oeschger events 9–13. Science 301, 1365–1367.

Burns, S.J., Fleitmann, D., Matter, A., Kramers, J., Al-Subbary, A.A., 2004. Indian Ocean climate and an absolute chronology over Dansgaard/Oeschger events 9–13: correction. Science 305, 1567.

Caley, T., Malaizé, B., Revel, M., Ducassou, E., Wainer, K., Ibrahim, M., Shoeaib, D., Migeon, S., Marieu, V., 2011a. Orbital timing of the Indian, East Asian and African boreal monsoons and the concept of a 'global monsoon'. Quaternary Science Reviews 30, 3705–3715.

Caley, T., Malaizé, B., Zaragosi, S., Rossignol, L., Bourget, J., Eynaud, F., Martinez, P., Giraudeau, J., Charlier, K., Ellouz-Zimmermann, N., 2011b. New Arabian Sea records help decipher orbital timing of Indo-Asian monsoon. Earth and Planetary Science Letters 308, 433–444.

Caley, T., Malaizé, B., Bassinot, F., Clemens, S.C., Caillon, N., Rossignol, L., Charlier, K., Rebaubier, H., 2011c. The monsoon imprint during the 'atypical' MIS 13 as seen through north and equatorial Indian Ocean records. Quaternary Research 76, 285–293.

Caley, T., Malaizé, B., Kageyama, M., Landais, A., Masson-Delmotte, V., 2013. Bihemispheric forcing of the Indo-Asian monsoon during glacial terminations. Quaternary Science Reviews 59, 1–4.

Chen, M.-T., 1994. Late Quaternary Paleoceanography of the Equatorial Indo-pacific Ocean: a Quantitative Analysis Based on Marine Micropaleontological Data. PhD thesis. Department of Geological Sciences, Brown University.

Chen, M.-T., Farrell, J., 1991. Planktonic foraminifer faunal variations in the northeastern Indian Ocean: a high-resolution record of the past 800,000 years from site 758. In: Weissel, J., Peirce, J., Tayor, E., Alt, J., et al. (Eds.), Proceedings of the ODP, Scientific Results, vol. 121. Ocean Drilling Program, College Station, Texas, pp. 125–140.

Chen, M.-T., Shiau, L.-J., Yu, P.-S., Chiu, T.-C., Chen, Y.-G., Wei, K.-Y., 2003. 500,000-year records of carbonate, organic carbon, and foraminiferal sea-surface temperature from the southeastern South China Sea (near Palawan Island). Palaeogeography, Palaeoclimatology, Palaeoecology 197, 113–131.

Cheng, H., Edwards, R.L., Wang, Kong, X., Ming, Y., Kelly, M.J., Wang, X., Gallup, C.D., Liu, W., 2006. A penultimate glacial monsoon record from Hulu Cave and two phase glacial terminations. Geology 34, 217–220.

Cheng, H., Edwards, R.L., Broecker, W.S., Denton, G.H., Kong, X., Wang, Y., Zhang, R., Wang, X., 2009. Ice age terminations. Science 326, 248–252.

Clemens, S.C., Prell, W., 1990. Late Pleistocene variability of Arabian Sea summer monsoon winds and continental aridity: Eolian records from the lithogenic component of deep-sea sediments. Paleoceanography 5, 109–145.

Clemens, S.C., Prell, W., Murray, D., Shimmield, G., Weedon, G., 1991. Forcing mechanisms of the Indian Ocean monsoon. Nature 353, 720–725.

Clemens, S.C., Murray, D.W., Prell, W.L., 1996. Nonstationary phase of the Plio–Pleistocene Asian monsoon. Science 274, 943–948.

Clemens, S.C., Prell, W.L., 2003. A 350,000 year summer-monsoon multi-proxy stack from the Owen Ridge, Northern Arabian Sea. Marine Geology 201, 35–51.

Clemens, S.C., Prell, W., 2007. The timing of orbital-scale Indian monsoon changes. Quaternary Science Reviews 26, 275–278.

Clemens, S.C., Prell, W., Sun, Y., Liu, Z., Chen, G., 2008. Southern hemisphere forcing of Pliocene delta $\delta^{18}O$ and the evolution of Indo-Asian monsoons. Paleoceanography 23, PA4210. http://dx.doi.org/10.1029/2008PA001638.

Clemens, S.C., Prell, W.L., Sun, Y., 2010. Orbital-scale timing and mechanisms driving Indo-Asian summer monsoons: reinterpreting speleothem $\delta^{18}O$. Paleoceanography 25, PA4207. http://dx.doi.org/10.1029/2010PA001926.

Clement, A.C., Hall, A., Broccoli, A.J., 2004. The importance of precessional signals in the tropical climate. Climate Dynamics 22, 327–341.

Curry, W.B., Thunell, R.C., Honjo, S., 1983. Seasonal changes in the isotopic composition of planktonic foraminifera collected in Panama Basin sediment traps. Earth and Planetary Science Letters 64, 33–43.

Ding, Y., Chan, J.C.L., 2005. The East Asian summer monsoon: an overview. Meteorology and Atmospheric Physics 89, 117–142.

Fairbanks, R.G., Wiere, P.H., Be, A.W.H., 1980. Vertical distribution and isotopic composition of living planktonic foraminifera in the western North Atlantic. Science 207, 61–63.

Fairbanks, R.G., Sverdlove, M., Free, R., Wiebe, P.H., Be, A.W.H., 1982. Vertican distribution and isotopic fractionation of living planktonic foraminifera from the Panama Basin. Nature 298, 841–844.
Field, D.B., 2004. Variability in vertical distributions of planktonic foraminifera in the California current: relationship to vertical ocean structure. Paleoceanography 19, PA2014. http://dx.doi.org/10.1029/2003PA000970.
Gadgil, S., 2003. The Indian monsoon and its variability. Annual Review of Earth and Planetary Sciences 31, 429–467.
Gadgil, S., Rajeevan, M., Francis, P.A., 2007. Monsoon variability: links to major oscillations over the equatorial Pacific and Indian oceans. Current Science 93, 182–194.
Ghil, M., Allen, M.R., Dettinger, M.D., Ide, K., Kondrashov, D., Mann, M.E., Robertson, A.W., Saunders, A., Tian, Y., Varadi, F., Yiou, P., 2002. Advanced spectral methods for climatic time series. Reviews of Geophysics 40, 1003.
Goswami, B.N., Madhusoodanan, M.S., Neema, C.P., Sengupta, D., 2006. A physical mechanism for North Atlantic SST influence on the Indian summer monsoon. Geophysical Research Letters 33, LO2706.
Govil, P., Naidu, P.D., 2010. Evaporation–precipitation changes in the eastern Arabian Sea for the last 68 ka: implications for monsoon variability. Paleoceanography 25, PA1210. http://dx.doi.org/10.1029/2008PA001687.
Gupta, A.K., Anderson, D.M., Overpeck, J.T., 2003. Abrupt changes in the Asian southwest monsoon during the Holocene and their links to the North Atlantic Ocean. Nature 421, 354–357.
Gupta, A.K., Mélice, J.-L., 2003. Orbital forcing of the Plio–Pleistocene Indian monsoons: benthic foraminiferal proxies from ODP Site 758. Current Science 85, 179–184.
Hemleben, C., Spindler, M., Anderson, O.R., 1989. Modern Planktonic Foraminifera. Springer, New York, p. 363.
Hodell, D.A., Channell, J.E.T., Curtis, J.H., Romero, O.E., Rohl, U., 2008. Onset of "Hudson Strait" Heinrich events in the eastern North Atlantic at the end of the middle Pleistocene transition (640 ka)? Paleoceanography 23, PA4218 http://dx.doi.org/10.1029/2008PA001591.
Howell, P., Pisias, N., Ballance, J., Baughman, J., Ochs, L., 2006. ARAND Time-series Analysis Software. Brown University, Providence RI.
Huybers, P., 2006. Early Pleistocene glacial cycles and the integrated summer insolation forcing. Science 313, 508–511.
Ishikawa, S., Oda, M., 2007. Reconstruction of Indian monsoon variability over the past 230,000 years: planktic foraminiferal evidence from the NW Arabian Sea open-ocean upwelling area. Marine Micropaleontology 63, 143–154.
Jin, L., Chen, F., Ganopolski, A., Claussen, M., 2007. Response of East Asian climate to Dansgaard/Oeschger and Heinrich events in a coupled model of intermediate complexity. Journal of Geophysical Research 112, D06117. http://dx.doi.org/10.1029/2006JD007316.
Kim, S.-T., O'Neil, J.R., 1997. Equilibrium and non-equilibrium oxygen isotope effects in synthetic carbonates. Geochimica y Cosmochimica Acta 61, 3461–3475.
Krishnamurti, T.N., 1985. Summer monsoon experiment: a review. Monthly Weather Review 113, 1590–1626.
Kroopnick, P., 1974. Correlations between ^{13}C and ΣCO_2 in surface waters and atmospheric CO_2. Earth and Planetary Science Letters 22, 397–403.
Kudrass, H.R., Hoffman, A., Doose, H., Emeis, K., Erlenkeuser, H., 2001. Modulation and amplification of climatic changes in the Northern hemisphere by the Indian summer monsoon during the past 80 k.y. Geology 29, 63–66.
Kutzbach, J.E., Prell, W., Ruddiman, W.F., 1993. Sensitivity of Eurasian climate to surface uplift of the Tibetan Plateau. Journal of Geology 101, 177–190.
Kutzbach, J.E., Liu, X., Liu, Z., Chen, C., 2008. Simulation of the evolutionary response of global summer monsoons to orbital forcing over the past 280,000 years. Climate Dynamics 30, 567–579.
Laskar, J., Joutel, F., Boudin, F., 1993. Orbital, precessional, and insolation quantities for the Earth from −20 Myr to +10 Myr. Astronomy and Astrophysics 270, 522–533.
Leduc, G., Vidal, L., Tachikawa, K., Bard, E., 2010. Changes in Eastern Pacific ocean ventilation at intermediate depth over the last 150 ka BP. Earth and Planetary Science Letters 298, 217–228.
Leuschner, D.C., Sirocko, F., 2003. Orbital insolation forcing of the Indian Monsoon – a motor for global climate changes? Palaeogeography, Palaeoclimatology, Palaeoecology 197, 83–95.
Levermann, A., Schewe, J., Petoukhov, V., Held, H., 2009. Basic mechanisms for abrupt monsoon transitions. Proceedings of the National Academy of Sciences USA 106, 20573–20577.
Lisiecki, L.E., Raymo, M.E., 2005. A Pliocene–Pleistocene stack of 57 globally distributed benthic delta-18 O records. Paleoceanography 20, PA1003. http://dx.doi.org/10.1029/2004PA001071.
Locarnini, R.A., Mishonov, A.V., Antonov, J.I., Boyer, T.P., Garcia, H.E., Baranova, O.K., Zweng, M.M., Johnson, D.R., 2010. World ocean atlas 2009. In: Levitus, S. (Ed.), Temperature, vol. 1. Government Printing Office, Washington, D.C., p. 184. NOAA Atlas NESDIS 68.
Masson, V., Braconnot, P., Jouzel, J., de Noblet, N., Cheddadi, R., Marchal, O., 2000. Simulation of intense monsoons under glacial conditions. Geophysical Research Letters 27, 1747–1750.
Mohtadi, M., Steinke, S., Groeneveld, J., Fink, H.G., Rixen, T., Hebbeln, D., Donner, B., Herunadi, B., 2009. Low-latitude control on seasonal and interannual changes in planktonic foraminiferal flux and shell geochemistry off south Java: a sediment trap study. Paleoceanography 24, PA1201. http://dx.doi.org/10.1029/2008PA001636.
Mohtadi, M., Oppo, D.W., Lückge, A., DePol-Holz, R., Steinke, S., Groeneveld, J., Hemme, N., Hebbeln, D., 2011. Reconstructing the thermal structure of the upper ocean: insights from planktic foraminifera shell chemistry and alkenones in modern sediments of the tropical eastern Indian Ocean. Paleoceanography 26, PA3219. http://dx.doi.org/10.1029/2011PA002132.
Molfino, B., McIntyre, A., 1990. Precessional forcing of nutricline dynamics in the Equatorial Atlantic. Science 249, 766–769.
Morley, J.J., Heusser, L.E., 1997. Role of orbital forcing in east Asian monsoon climates during the last 350 kyr: evidence from terrestrial and marine climate proxies from core RC14-99. Paleoceanography 12, 483–494. http://dx.doi.org/10.1029/97PA00213.
Oppenheimer, C., 2002. Limited global change due to the largest known Quaternary eruption, Toba ~74 kyr BP? Quaternary Science Reviews 21, 1593–1609.
Paillard, D., Labeyrie, L., Yiou, P., 1996. Macintosh program performs time-series analysis. Eos Transactions American Geophysical Union 77, 379.
Pausata, F.S.R., Battisti, D.S., Nisancioglu, K.H., Bitz, C.M., 2011. Chinese stalagmite $\delta^{18}O$ controlled by changes in the Indian monsoon during a simulated Heinrich event. Nature Geoscience 4, 474–480.
Pena, L.D., Cacho, I., Ferretti, P., Hall, M.A., 2008. El Niño-southern oscillation-like variability during glacial terminations and interlatitudinal teleconnections. Paleoceanography 23, PA3101. http://dx.doi.org/10.1029/2008PA001620.
Porter, S.C., An, Z.S., 1995. Correlation between climate events in the North Atlantic and China during the last glaciation. Nature 375, 305–308.
Prell, W.L., 1984. Monsoonal climate of the Arabian Sea during the Late Quaternary: a response to changing solar radiation. In: Berger, A.L., Imbrie, J., Hays, J., Kukla, G., Saltzman, B. (Eds.), Milankovitch and Climate. D. Riedel, Hingham, pp. 349–366.
Prell, W., Niitsuma, N., et al., 1989. In: Proceedings of the Ocean Drilling Program, Initial Reports, vol. 117. Ocean Drilling Program, College Station, Texas.
Prell, W., Kutzbach, J.E., 1992. Sensitivity of the Indian Monsoon to forcing parameters and implications for its evolution. Nature 360, 647–652.
Rachid, H., Flower, B.P., Poore, R.Z., Quinn, T.M., 2007. A ~25 ka Indian Ocean monsoon variability record from the Andaman Sea. Quaternary Science Reviews 26, 2586–2597.
Rachid, H., England, E., Thompson, L., Polyak, L., 2011. Late Glacial–Holocene Indian summer monsoon variability based upon sediment records taken from the Bay of Bengal. Terrestrial, Atmospheric and Oceanic Sciences 22, 215–228.
Ravelo, A.C., Shackleton, N.J., 1995. Evolution of surface water circulation in the east equatorial Pacific over the past 2.0 Ma: isotopic measurements from ODP Site 851. In: Pisias, N.G., Mayer, L.A., Janecek, T.R., Palmer-Julson, A., van Andel, T.H. (Eds.), Proceeding of the Ocean Drilling Program, Scientific Results, vol. 138. Ocean Drilling Program, College Station, Texas, pp. 503–514.
Reichart, G.J., Lourens, L.J., Zachariasse, J.W., 1998. Temporal variability in the northern Arabian Sea oxygen minimum zone (OMZ) during the last 225,000 years. Paleoceanography 13, 607–621. http://dx.doi.org/10.1029/98PA02203.
Roberts, A.P., Rohling, E.J., Grant, K.M., Larrasoaña, J.C., Liu, Q., 2011. Atmospheric dust variability from Arabia and China over the last 500,000 years. Quaternary Science Reviews 30, 3537–3541.
Rohling, E.J., Mayewski, P.A., Challenor, P., 2003. On the timing and mechanism of millennial-scale variability during the last glacial cycle. Climate Dynamics 20, 257–267.
Rohling, E.J., Sprovieri, M., Cane, T., Casford, J.S.L., Cooke, S., Bouloubassi, I., Emeis, K.C., Schiebel, R., Rogerson, M., Hayes, A., Jorissen, F.J., Kroon, D., 2004. Reconstructing past planktic foraminiferal depth habitats using stable isotope data: a case history for Mediterranean sapropel S5. Marine Micropaleontology 50, 89–123.
Rohling, E.J., Grant, K., Bolshaw, M., Roberts, A.P., Siddall, M., Hemleben, C., Kucera, M., 2009a. Antarctic temperature and global sea level closely coupled over the past five glacial cycles. Nature Geoscience 2, 500–504.
Rohling, E.J., Liu, Q.S., Roberts, A.P., Stanford, J.D., Rasmussen, S.O., Langen, P.L., Siddall, M., 2009b. Controls on the East Asian monsoon during the last glacial cycle, based on comparison between Hulu Cave and polar ice-core records. Quaternary Science Reviews 28, 3291–3302.
Rohling, E.J., Braun, K., Grant, K., Kucera, M., Roberts, A.P., Siddall, M., Trommer, G., 2010. Comparison between Holocene and Marine Isotope Stage-11 sea-level histories. Earth and Planetary Science Letters 291, 97–105.
Ruddiman, W.F., 2006. What is the timing of orbital-scale monsoon changes? Quaternary Science Reviews 25, 657–658.
Schmuker, B., Schiebel, R., 2002. Planktic foraminifers and hydrography of the eastern and northern Caribbean Sea. Marine Micropaleontology 46, 387–403.
Schott, F., McCreary, J.P., 2001. The monsoon circulation of the Indian Ocean. Progress in Oceanography 51, 1–123.
Schulz, H., von Rad, U., Erlenkeuser, H., 1998. Correlation between Arabian sea and Greenland climate oscillations of the past 110,000 years. Nature 393, 54–57.
Shackleton, N.J., Hall, M.A., 1984. Oxygen and Carbon Isotope Stratigraphy of Deep Sea Drilling Project Hole 552A: Plio–pleistocene Glacial History. Initial Reports of the Deep Sea Drilling Project, pp. 599–609.
Shankar, D., Vinayachandran, P.N., Unnikrishnan, A.S., Shetye, S.R., 2002. The monsoon currents in the north Indian Ocean. Progress in Oceanography 52, 63–119.
Shipboard Scientific Party, 1989. Site 758. In: Peirce, J., Weissel, J., et al. (Eds.), Proceedings of the Ocean Drilling Program, Initial Reports, vol. 121, pp. 359–453. College Station, Texas.
Spero, H.J., Lea, D.W., 1996. Experimental determination of stable isotope variability in *Globigerina bulloides*: implications for paleoceanographic reconstructions. Marine Micropaleontology 28, 231–246.

Spero, H.J., Bijma, J., Lea, D.W., Bemis, B.E., 1997. Effect of seawater carbonate concentration on foraminiferal carbon and oxygen isotopes. Nature 390, 497–500.
Spero, H.J., Mielke, K.M., Kalve, E.M., Lea, D.W., Pak, D.K., 2003. Multispecies approach to reconstructing eastern equatorial Pacific thermocline hydrography during the past 360 kyr. Paleoceanography 18 (1), 1022. http://dx.doi.org/10.1029/2002PA000814.
Steinke, S., Mohtadi, M., Groeneveld, J., Lin, L.-C., Löwemark, L., Chen, M.-T., Rendle-Bühring, R., 2010. Reconstructing the southern South China Sea upper water column structure since the Last Glacial Maximum: implications for the East Asian winter monsoon development. Paleoceanography 25, PA2219. http://dx.doi.org/10.1029/2009PA001850.
Steph, S., Regenberg, M., Tiedemann, R., Mulitza, S., Nürnberg, D., 2009. Stable isotopes of planktonic foraminifera from tropical Atlantic/Caribbean coretops: implications for reconstructing upper ocean stratification. Marine Micropaleontology 71, 1–19.
Steph, S., Tiedemann, R., Prange, M., Groeneveld, J., Schulz, M., Timmermann, A., Nürnberg, D., Rühlemann, C., Saukel, C., Haug, G.H., 2010. Early Pliocene increase in thermohaline overturning: a precondition for the development of the modern equatorial Pacific cold tongue. Paleoceanography 25, PA2202. http://dx.doi.org/10.1029/2008PA001645.
Sun, J., Huang, X., 2006. Half-precession cycles recorded in Chinese loess: response to low-latitude insolation forcing during the Last Interglaciation. Quaternary Science Reviews 25, 1065–1072.
Sun, Y., Clemens, S.C., An, Z., Yu, Z., 2006. Astronomical timescale and paleoclimatic implication of stacked 3.6-Myr monsoon records from the Chinese Loess Plateau. Quaternary Science Reviews 25, 33–48.
Verschuren, D., Sinninghe Damsté, J.S., Moernaut, J., Kristen, I., Blaauw, M., Fagot, M., Haug, G.H., CHALLACEA project members, 2009. Half-precessional dynamics of monsoon rainfall near the East African Equator. Nature 462, 637–641.
Wang, B., Clemens, S.C., Liu, P., 2003a. Contrasting the Indian and East Asian monsoons: implications of geologic timescales. Marine Geology 201, 5–21.
Wang, L., 2000. Isotopic signals in two morphotypes of *Globigerinoides ruber* (white) from the South China Sea: implications for monsoon climate change during the last glacial cycle. Palaeogeography, Palaeoclimatology, Palaeoecology 161, 381–394.
Wang, P., Jian, Z., Zhao, Q., Li, Q., Wang, R., Liu, Z., Wu, G., Shao, L., Wang, J., Huang, B., Fang, D., Tian, J., Li, J., Li, X., Wei, G., Sun, X., Luo, Y., Su, X., Mao, S., Chen, M., 2003b. Evolution of the South China Sea and monsoon history revealed in deep-sea records. Chinese Science Bulletin 48, 2549–2561.
Wang, P., Clemens, S.C., Beaufort, L., Braconnot, P., Ganssen, G., Jian, Z., Kershaw, P., Sarnthein, M., 2005. Evolution and variability of the Asian monsoon system: state of the art and outstanding issues. Quaternary Science Reviews 24, 595–629.
Wang, Y.J., Cheng, H., Edwards, R.L., An, Z.S., Wu, J.Y., Shen, C.-C., Dorale, J.A., 2001. A high-resolution absolute-dated late Pleistocene monsoon record from Hulu Cave, China. Science 294, 2345–2348.
Wang, Y.J., Cheng, H., Edwards, R.L., Kong, X., Shao, X., Chen, S., Wu, J., Jiang, X., Wang, X., An, Z., 2008. Millennial-band orbital-scale changes in the east Asian monsoon over the past 224,000 years. Nature 451, 1090–1093.
Weber, S.L., Tuenter, E., 2011. The impact of varying ice sheets and greenhouse gases on the intensity and timing of boreal summer monsoons. Quaternary Science Reviews 30, 469–479.
Webster, P.J., 1987. The elementary monsoon. In: Fein, J.S., Stephens, P.L. (Eds.), Monsoons. John Wiley, New York, pp. 3–32.
Webster, P.J., Magafia, V.O., Palmer, T.N., Shukla, J., Tomas, R.A., Yanai, M., Yasunari, T., 1998. Monsoons: processes, predictability and the prospects for prediction. Journal of Geophysical Research 103, 14451–14510.
Wright, H.T.J., Kutzback, J.E., Webb III, T., Ruddiman, W.F., Street-Perrott, F.A., Bartlein, P.J. (Eds.), 1993. Global Climates Since the Last Glacial Maximum. University of Minnesota Press, Minneapolis, p. 569.
Zhou, H., Zhao, J., Feng, Y., Gagan, M.K., Zhou, G., Yan, J., 2008. Distinct climate change synchronous with Heinrich event one, recorded by stable oxygen and carbon isotopic compositions in stalagmites from China. Quaternary Science Reviews 69, 306–315.
Ziegler, M., Lourens, L.J., Tuenter, E., Hilgen, F., Reichart, G.J., Weber, N., 2010. Precession phasing offset between Indian summer monsoon and Arabian Sea productivity linked to changes in Atlantic overturning circulation. Paleoceanography 25, PA3213. http://dx.doi.org/10.1029/2009PA001884.